Discontinuous transitions of social distancing in the SIR model

R. Arazi, A. Feigel *

Racah Institute of Physics, The Hebrew University, 9190401 Jerusalem, Israel

ARTICLE INFO

ABSTRACT

To describe the dynamics of social distancing during pandemics, we follow previous efforts to combine basic epidemiology models (e.g. SIR — Susceptible, Infected, and Recovered) with game and economic theory tools. We present an extension of the SIR model that predicts a series of discontinuous transitions in social distancing. Each transition resembles a phase transition of the second-order (Ginzburg–Landau instability) and, therefore, potentially a general phenomenon. The first wave of COVID-19 led to social distancing around the globe: severe lockdowns to stop the pandemic were followed by a series of lockdown lifts. Data analysis of the first wave in Austria, Israel, and Germany corroborates the soundness of the model. Furthermore, this work presents analytical tools to analyze pandemic waves, which may be extended to calculate derivatives of giant components in network percolation transitions and may also be of interest in the context of crisis formation theories.

© 2020 Elsevier B.V. All rights reserved.

1. Introduction

Pandemics are complex medical and socioeconomic phenomena [1]: frequent social interactions benefit both the spread of disease and significant parts of modern economics [2,3]. Rational human behavior during pandemics suggests a balance between individual efforts to avoid getting infected and the economic costs of protective measures [4,5]. This balance changes with time and disease prevalence [6]. This work argues that this balance, together with the corresponding human behavior, may possess discontinuous transitions similar to the free energy of a system during the Ginzburg–Landau phase transition and may have some level of universality [7–11].

Social distancing is an effective tool to mitigate disease transmission [2,3]. It consists of self or government-imposed constraints on interpersonal contacts. Social distancing, however, comes at a significant economic cost in terms of reduced productivity [4,12].

Social distancing depends on epidemic dynamics and vice versa [1,6,13,14]. Epidemic dynamics are known through daily-reported amounts of infected and deceased persons (see Fig. 1 for mortality due to Spanish flu in England and Wales) [15,16]. A graph like that shown in Fig. 1 should reflect changes in social distancing over time.

Some reports of confirmed cases or mortalities as the functions of time possess a kink soon after the epidemic peak, for instance, see the red point in Fig. 1. We will also see similar phenomena with COVID-19 data. The red point in Fig. 1 may indicate noise in reported data, changes in testing policy, responses to some extraneous phenomena, or a combination of two temporarily and spatially separated epidemic waves. On the other hand, one can put forward the hypothesis that it indicates an abrupt transition in social distancing practice as a response to reduced levels of the epidemic.

For example, consider a hypothesis that discontinuity in time derivative of reported mortalities (as shown by the red dot in Fig. 1) is a consequence of an abrupt change in social distancing. The population accepted significant social

---

* Corresponding author.
 E-mail address: sasha@phys.huji.ac.il (A. Feigel).

Fig. 1. Mortality in England and Wales during the second wave of Spanish flu. The red dot indicates a transition in time derivative soon after the epidemic peak. This work presents a theory that describes this type of transition as a rational decision regarding the optimal value of social distancing in a population. The theory predicts discontinuous, phase transition-like, changes in social distancing. We do not claim that this work provides the only possible explanation of the discontinuous time derivatives of epidemic dynamics.

distancing at the beginning of the wave but increasingly rejected it after the pandemic passed its peak. To estimate the time and strength of transition, one needs an epidemiological model that includes human behavior.

The SIR model [17] separates the population into three compartments: susceptible, infected and recovered. The flux between these compartments goes in the order susceptible $\rightarrow$ infected $\rightarrow$ recovered, since susceptible people may become infected during encounters with infected individuals. Newly-infected people stay contagious for some time, after which they stop spreading the disease and become immune (recover) or die. The population is well mixed and sustains the gas-like interaction of its members.

This work follows many previous efforts to investigate the role of human behavior during an epidemic [6,13,18–22]. Parameters of the SIR model [17] can depend on disease prevalence [6], be time dependent [23], include spatial effects [24,25], be more elaborated by the separation of the susceptible and infected into sub-compartments [26], include adaptive mobility [27], or include information-related contact patterns [28–30]. Specifically, we have made modifications to the SIR model with economic tools [3–5,31–36] and game theory methods [37–39]. Policy [40] and pandemic management is out of the scope of this work.

To proceed, one should associate social distancing with a parameter of an epidemiological model. Following many previous studies, we will choose basic reproduction number R_0 as a measure of both social distancing and its economic cost [20,39,41–44].

Basic reproduction number R_0 is the expected number of infected directly generated by one infected person in a population where all individuals are susceptible to infection [45]. R_0 is a measure of social distancing because it is proportional to the frequency of interpersonal interactions. The economic cost of social distancing, therefore, can be considered as a function of R_0 [44]. Further, in this work, for the sake of convenience, we will use the inverse of the basic reproduction number $s_{th} = 1/R_0$ as the main parameter: epidemic breaks out only if $R_0 > 0$, thus s_{th} is bounded $0 < s_{th} < 1$.

In this work, changes in the value of $s_{th} = 1/R_0$, $s_{th}^{(0)} \rightarrow s_{th}^{(1)}$ correspond to the balance between changes in the final epidemic size FES (the number of new infections from the current moment till the end of epidemic) [46,47] and changes in economic cost EC [44]:

$$FES(s_{th}^{(1)}, t) - FES(s_{th}^{(0)}, t) = EC(s_{th}^{(1)}, t) - EC(s_{th}^{(0)}, t). \tag{1}$$

Both FES and EC are defined at time t when individuals (or the government) make their decision. This time, however, is a function of the subsequent sequence of trajectories of individual decisions.

A major assumption of this work is that decisions regarding transition $s_{th}^{(0)} \rightarrow s_{th}^{(1)}$ consider only two possible future trajectories: either $s_{th}^{(0)}$ or $s_{th}^{(1)}$ and these remain constant until the end of the epidemic. Otherwise, FES cannot be considered entirely as a function of the single value of s_{th}.

The extension of (1) in the Taylor series of Δs_{th} results in a non-linear expression similar to the free energy of a system with Ginzburg–Landau instability.

This work proceeds with the presentation of the SIR model with induced transitions (SIRIT), an almost analytical treatment of this model, the calibration of the epidemiological and economic parameters of the model (using a time series of confirmed cases and causalities during the first wave of COVID-19 in Austria, Israel, and Germany), followed by a discussion of the obtained results and their implications.

2. Discontinuous transitions in the SIR model with utility function

Here are the SIR model's equations that describe the spread of a disease in a population:

$$\frac{\partial s}{\partial t} = -\beta i s,$$

$$\frac{\partial i}{\partial t} = \beta i s - \gamma i, \tag{2}$$

$$\frac{\partial r}{\partial t} = \gamma i$$

where $s(t)$, $i(t)$, and $r(t)$ are the fractions of the population in the susceptible, infected, and recovered states respectively. The third equation is redundant since $s + i + r = 1$. Rate β includes both the rate of interaction between population members and the probability of disease transmission during these interactions. An infected person is contagious for a period of time having average duration γ^{-1}.

Both β and γ may represent changes in human behavior that affect the spread of disease. The frequency of social interactions and the level of self-protection define β. During severe pandemics like COVID-19, human or government decisions also affect γ by contact tracing and self or government-imposed quarantine of individuals who are known or suspected to be infected.

If rates β and γ are constant in time, Eqs. (2) reduce to:

$$\frac{\partial s}{\partial t^*} = -si,$$

$$\frac{\partial i}{\partial t^*} = i\left(s - \frac{1}{R_0}\right) = i\left(s - s_{th}\right), \tag{3}$$

where $t^* = \beta t$ is dimensionless time and $R_0 = \beta/\gamma$ is basic reproduction number − the expected number of infections directly generated by one infected person in a population where all individuals are susceptible to infection [45]. In addition, R_0 defines the threshold ratio of susceptible s_{th} that defines the course of the epidemic: the number of infected increase if $s > s_{th}$ and decrease if $s < s_{th}$. We will use s_{th}, rather than R_0, as the main parameter in this work.

Eq. (3) possesses a solution in (s, i) space, see Fig. 2 and Appendix A. The form of the trajectory (s_t, i_t) depends only on initial values $s_{th}^{(0)}$ and (s_0, i_0). The trajectory starts at (s_0, i_0) and advances to $(s_{min}, 0)$. The amount of infected people reaches its maximum value at $s = s_{th}^{(0)}$.

To calculate transition:

$$s_{th}^{(0)} \to s_{th}^{(1)}, \tag{4}$$

following (1), we introduce the utility function:

$$U(s_{th}, t) = -FES(s_{th}, t) + EC(s_{th}, t), \tag{5}$$

where the final epidemic size FES is:

$$FES = \int_t^\infty i \, dt^*. \tag{6}$$

and economic cost is some unknown function $EC(s_{th}, t)$. The utility function and its components FES and EC can be considered as functions of s rather than time t in (s, i) space.

In this work, we consider only the relaxation of social distancing. At each moment t the value of $s_{th}^{(0)}$ changes if there exists $s_{th}^{(1)} < s_{th}^{(0)}$ such that:

$$U(s_{th}^{(1)}, t) - U(s_{th}^{(0)}, t) > 0. \tag{7}$$

Both FES and EC are defined at the time t of transition.

To calculate $s_{th}^{(1)}$ let us expand U into a Taylor series. Specifically, let us expand EC to the second order and FES to the third order of s_{th}, because FES prevents large changes in s_{th} (a return to the pre-pandemic level of social distancing).

Economic cost is a general unknown function $EC(s_{th}, t)$. We assume that at each time t it possesses a Taylor expansion:

$$EC(s_{th} + \Delta s_{th}, t) = EC(s_{th}, t) - E^{(1)} \Delta s_{th} + E^{(2)} \Delta s_{th}^2. \tag{8}$$

The choice of the signs in (8) assures that $E^{(1)}$ and $E^{(2)}$ are positive for $\Delta s_{th} < 0$. We also assume that parameters $E^{(1)}$ and $E^{(2)}$:

$$E^{(1)} = -\frac{\partial EC}{\partial s_{th}}, \quad E^{(2)} = \frac{1}{2}\frac{\partial^2 EC}{\partial s_{th}^2}, \tag{9}$$

are constant and define the economic cost of changes in s_{th}.

The Taylor expansion of final epidemic size (6) is:

$$FES(s_{th} + \Delta s_{th}, t) =$$
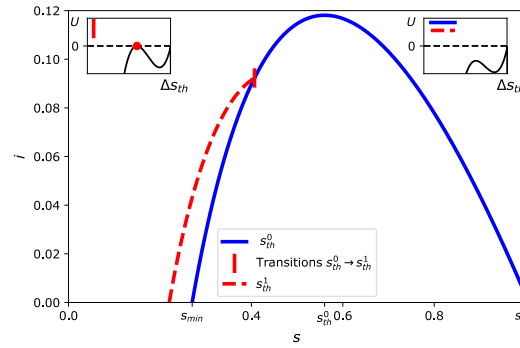$$FES(s_{th}, t) + F^{(1)} \Delta s_{th} + F^{(2)} \Delta s_{th}^2 + + F^{(3)} \Delta s_{th}^3. \tag{10}$$

Fig. 2. Single transition $s_{th}^{(0)} \rightarrow s_{th}^{(1)}$. The SIR model trajectory in (s, i) space without transition (solid blue). Trajectory starts at $(s_0 \approx 1, i_0 \approx 0)$. The ratio of susceptible people s in the population reduces. The ratio of infected people i increases for $s > s_{th}^{(0)}$ and decreases for $s < s_{th}^{(0)}$. Before transition (red bar), utility function $U < 0$ for any $s_{th} < s_{th}^{(0)}$. At transition the utility function possesses single value $s_{th}^{(1)}$ such that $U(s_{th}^{(1)}) = 0$. Then transition $s_{th}^{(0)} \rightarrow s_{th}^{(1)}$ takes place. Immediately after transition again $U < 0$ for any $s_{th} < s_{th}^{(1)}$. The trajectory with transition (dashed red) converges to $s_{min}^{(1)}$ which is lower than s_{min} of the original trajectory.
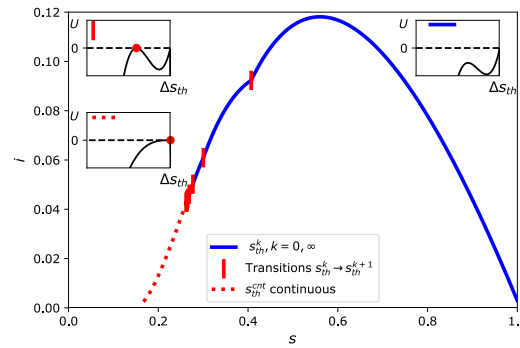

Fig. 3. Multiple transitions $s_{th}^{(0)} \rightarrow s_{th}^{(1)} \rightarrow s_{th}^{(2)} \rightarrow \cdots \rightarrow s_{th}^{(k)} \cdots \rightarrow s_{th}^{\infty}$. Conditions $U(s_{th}^{(k+1)}) = 0$ for $s_{th}^{(k+1)} < s_{th}^{(k)}$ keep hold along the trajectory of the SIR model in (s, i) space. This results in a series of discontinuous transitions (red bars) that eventually converge to some limit values s_{tr}^{lim} and s_{th}^{lim}. The time that it takes to pass all these infinite number of transitions is finite, as it is any time between the two values of $s > s_{min}$. This results in a Zeno-like phenomenon. The final value of s_{th}^{lim} depend on $s_0, i_0, s_{th}^{(0)}$ and the parameters of economic cost $E^{(1)}$ and $E^{(2)}$. For $s < s_{tr}^{lim}$ s_{th} changes continuously (dotted red), with a utility function that at each moment predicts transition $\Delta s_{th} = 0$.

where:

$$F^{(1)} = \frac{\partial FES}{\partial s_{th}}, F^{(2)} = \frac{1}{2} \frac{\partial^2 FES}{\partial s_{th}^2}, F^{(3)} = \frac{1}{6} \frac{\partial^3 FES}{\partial s_{th}^2}. \tag{11}$$

$F^{(1)}$, $F^{(2)}$ and $F^{(3)}$ depend on position along the trajectory (s_t, i_t).

Coefficients $F^{(1)}$, $F^{(2)}$ and $F^{(3)}$ can be derived as analytical functions of s_t and $s_{th}^{(0)}$. Following (3) and (6), FES at any time t is:

$$FES = \log s_{min} - \log s_t, \tag{12}$$

Thus $F^{(1)}$, $F^{(2)}$ and $F^{(3)}$ are derivatives of s_{min} due to s_{th}. s_{min} can be expressed using the Lambert W function [48–51]:

$$s_{min} = -s_{th}^{(0)} W \left(-\frac{s_0}{s_{th}^{(0)}} \exp \left[-\frac{i_0 + s_0}{s_{th}^{(0)}} \right] \right). \tag{13}$$

Derivatives of the Lambert W function can be calculated analytically. s_{min} does not change along the trajectory, thus at any time before transition one can change $(s_0, i_0) \rightarrow (i_t, s_t)$. Derivatives of s_{min} due to s_{th} depend on (s_t, i_t). Finally, $F^{(1)}$, $F^{(2)}$, and $F^{(3)}$ are functions of s_t and s_{th}, (see Appendix B).

The main proposition of this work is that utility function (5) possesses Ginzburg–Landau-like instability, see Fig. 4. The utility function (5), taking into account (8) and (10), is $U(s_{th} + \Delta s_{th}) = U(s_{th}) + \Delta U$ where:

$$\Delta U = -(F^{(1)} + E^{(1)}) \Delta s_{th} - (F^{(2)} - E^{(2)}) \Delta s_{th}^2 - F^{(3)} \Delta s_{th}^3. \tag{14}$$
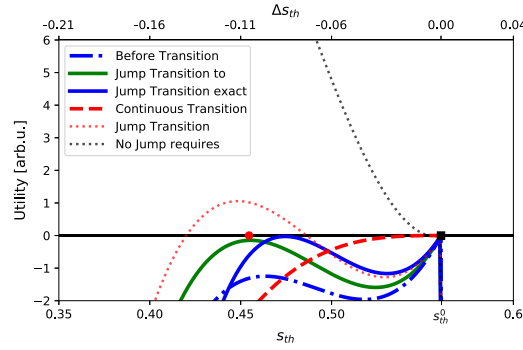
Fig. 4. Utility as a function of s_{th} before, during, and after transition takes place. A measure of social distancing is $0 < s_{th} < 1$. Transition occurs between current value of $s_{th}^{(0)}$ (black square) to its new value $s_{th}^{(1)}$ (red circle) when $U(s_{th}^{(1)}) > U(s_{th}^{(0)})$ ($U(s_{th}^{(0)}) = 0$). Before transition $U(s_{th}^{(0)})$ is the highest value of the utility function (dashed–dotted blue). Then there are two possibilities: discontinuous change $s_{th}^{(1)} \neq s_{th}^{(0)}$ (solid green line) or continuous change $s_{th}^{(1)} \approx s_{th}^{(0)}$ (dashed red line). Two cases (dotted lines) that make possible the change of s_{th} to many values do not exist because either continuous or discontinuous transition occurred before. This work considers only a reduction in the level of social distancing, which corresponds to a reduction of s_{th}. Utility function is approximately a cubic function of Δs_{th} (solid green). The transition predicted by the exact calculation (solid blue) for this work predict insignificant changes in the time and strength of the transition.

is the third-degree polynomial of Δs_{th}. First, no transition occurs if $\Delta U < 0$ for all $\Delta s_{th} < 0$. Second, discontinuous change in $s_{th}^{(0)} \to s_{th}^{(1)}$ takes place if there is single value $\Delta U(s_{th}) = 0$ for all $\Delta s_{th} < 0$. Third, s_{th} changes continuously when derivatives of (14) vanish near $\Delta s_{th} = 0$. To prevent transitions with $\Delta s_{th} > 0$ we assume that the economic cost of additional social distancing is high and overrides the potential reduction of *FES*.

Discontinuous transition occurs when there exists a single $\Delta s_{th} < 0$ root for $\Delta U = 0$ (14). This condition requires the determinant of quadratic function $U/\Delta s_{th}$ (14) to vanish:

$$4F^{(3)}(F^{(1)} + E^{(1)}) = (F^{(2)} - E^{(2)})^2. \tag{15}$$

This is the fourth-order polynomial of $\log s_t$ because $F^{(1)}$, $F^{(2)}$, and $F^{(3)}$ are polynomials of $\log s_t$ of the first, second, and third degrees correspondingly, see Appendix C.

Following (14), transition strength Δs_{th} is:

$$\Delta s_{th} = \frac{F^{(2)} - E^{(2)}}{2F^{(3)}}. \tag{16}$$

Then:

$$s_{th}^{(1)} = s_{th}^{(0)} + \Delta s_{th}, \tag{17}$$

is the new value of $s_{th}^{(0)}$.

To calculate when transition takes place on a trajectory $(s_{th}^{(0)}, s_0, i_0)$ one should solve the 4th order polynomial (15) for s_{tr} and take the closest to 0 negative root. One can use (16) to calculate new value $s_{th}^{(1)}$ and continue the trajectory $(s_{th}^{(1)}, s_{tr}, i(s_{tr}))$.

Previous results can be presented as two functions:

$$\begin{aligned}
s_{tr}^{(1)} &= T_1(s_0, i_0, s_{th}^{(0)}, E^{(1)}, E^{(2)}), \\
s_{th}^{(1)} &= T_2(s_0, i_0, s_{th}^{(0)}, E^{(1)}, E^{(2)}).
\end{aligned} \tag{18}$$

T_1 defines where transition takes place $s = s_{tr}^{(1)}$ while T_2 defines the transition strength $s_{th}^{(0)} \to s_{th}^{(1)}$.

Consider the single transition in Fig. 2. This trajectory consists of the points (s_t, i_t), starts at (s_0, i_0) and proceeds to lower values of s. At some moment condition (15) alarms and a new value of s_{th} appears.

For a single transition, one can consider an inverse problem − to calculate $E^{(1)}$ and $E^{(2)}$ if the transition position s_{tr} and its strength Δs_{th} are known.

The trajectory (s_t, i_t) may include multiple transitions. Condition (15) may occur after the first transition and so on. To calculate these transition one should repeatedly apply (18) with change $(s_{th}^{(k)}, s_k, i_k) \to (s_{th}^{(k+1)}, s_{k+1}, i_{k+1})$.

Many transitions (18) result in a Zeno-like phenomenon − the system makes an infinite number of transitions in a finite amount of time, see Fig. 5. Repeated application of T_1 and T_2 (18) results in convergence of s_{th} and s_{tr} to some limit values (s_{th}^{lim} and s_{lim} respectively). The time to reach s_{th}^{lim} is finite, as any time between the two values of $s > s_{min}$, see (A.3).

For $s < s_{tr}^{lim}$, the utility function preserves the continuous transition state. At s_{th}^{lim} (18) predicts $\Delta s_{th} = 0$, see Fig. 4. At the region of continuous transitions, at each moment equation:
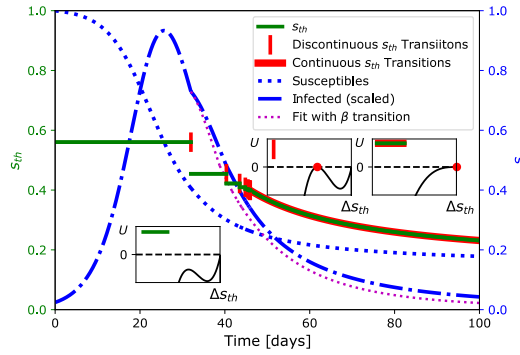
$$F^{(1)} = -E^{(1)} \tag{19}$$

Fig. 5. Epidemic wave dynamics with social distancing transitions. The SIR model predicts the wave-like behavior of infected individuals (dash-dotted blue) accompanied by a reduction in the number of susceptible people (dotted blue). A utility function causes changes in social distancing parameter s_{th} (solid green). Transition (red bars) occurs when there exists a new value of $s_{th}^{(1)}$ such that the utility function $U(s_{th}^{(1)}) > 0$. The forms of the utility function before and during the transition are shown in the subplots. A region of continuous transitions follows a series of discontinuous ones. Changes in s_{th} cause time derivative discontinuities in the dynamics of the infected and susceptible numbers. These are especially prominent in the first transition (outermost left red bar) soon after the epidemic's peak. In time-space population, trajectory depends on whether the change of $s_{th} = \gamma/\beta$ occurred by the change of γ (dashed–dotted blue) or β (dotted magenta). The difference is insignificant for this work.

defines s_{th}, and (3) is solved numerically. Otherwise, if s_{th} remains constant the utility function would make possible many values of s_{th} with $U(s_{th}) > 0$, see Fig. 4.

The single transition requires an assumption that the economic cost is a function of the basic reproduction number. For multiple transitions, we assume that economic cost is the same for all transitions. To check the validity of these and other assumption of the model we proceed to fit the first wave of COVID-19.

3. Fit

The main purpose of this section is to show that the model of discontinuous transitions of social distancing (see Section 2) may fit the first COVID-19 wave data. Full optimization of the COVID-19 data fit and its validation is out of the scope of this work. To proceed we want to make our model compatible with the COVID-19 data.

During the COVID-19 pandemic, there are daily worldwide reports [52] of confirmed cases and deaths. Confirmed cases are detected infections, which are a fraction of the total number of infected people. The ratio between confirmed and total COVID-19 cases is unknown and may vary from country to country or even change in time due to changes in test policies. Nevertheless, some countries may be similar to each other [53].

For the sake of the fit, first, we should introduce new parameters that represent unknowns of the data. Second, we should consider dynamics in time-space rather than (s, i) space.

Let us rewrite (2) as:

$$
\begin{aligned}
\frac{\partial s}{\partial t} &= -\beta A s I, \quad A = \frac{A'}{N}, \\
\frac{\partial I}{\partial t} &= \beta I(s - s_{th}), \\
\frac{\partial D}{\partial t} &= \beta s_{th} N A I M
\end{aligned}
\tag{20}
$$

where s remains to be fraction of susceptible, I reported confirmed cases and D is reported deaths due to the epidemic. A' is a ratio between actual and reported confirmed cases and N is the population size, thus $D = MNr$, where M is infected fatality rate (IFR). When population size N and A' remain constant it is convenient to unite them into a single parameter $A = \frac{A'}{N}$. Eqs. (20) converge to (2) if $A' = 1$, with the only difference being that the third equation addresses deceased instead of recovered. Parameter β and s_{th} are the same as in (2).

To proceed with a fit we assume that only those parameters that are related to human behavior can change with time, thus β and s_{th} change with time, while A', N, and M remain constant (these parameters relate to testing policies and disease clinics.). This choice fits our purpose to show that COVID-19 data can be explained by changes in social distancing. In reality, however, all parameters of the SIR model are continuous functions of time or the state of the epidemic. The implications of this assumption are addressed in the discussion Section 4.

See Fig. 5 for trajectory in time, corresponding to trajectory in (s, i) space in Fig. 3. The trajectory in time space depends on β and s_{th}, rather than only s_{th}. Thus transition $s_{th}^{(k)} \rightarrow s_{th}^{(k+1)}$ may be interpreted as a change in β, in γ or in both β and γ. Choosing every transition as a change in γ (dash-dotted blue) or change in β (dotted magenta) results in similar
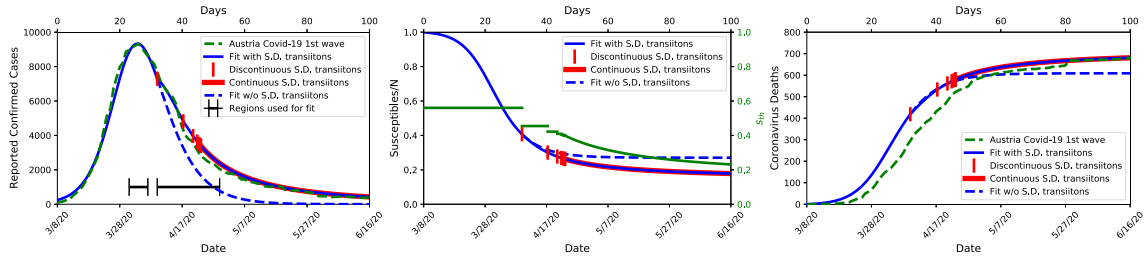
Fig. 6. Fit of Austria COVID-19 first wave with multiple social distancing transitions. The purpose of the fit is to show that there is a possibility to fit the real data using many transitions. (A) Confirmed cases − reported (dashed green) and calculated with many transitions (solid blue). Before transitions (red bars) classical SIR model fits well with the reported confirmed cases. There is a significant deviation of the SIR model from reported cases after the first transition (dashed blue). The SIRIT model with many transitions fits well with the entire range of the first wave, though the fit was obtained using a small range around the peak of confirmed cases and characteristics of the first transition (horizontal error bars). (B) Susceptible and social distance parameter s_{th}. At each transition s_{th} changes its value. A series of discontinuous transitions is followed by a continuous change region. (C) Coronavirus deaths. There exists a time delay between reported and calculated deaths. This delay can be explained by the long course of COVID-19.
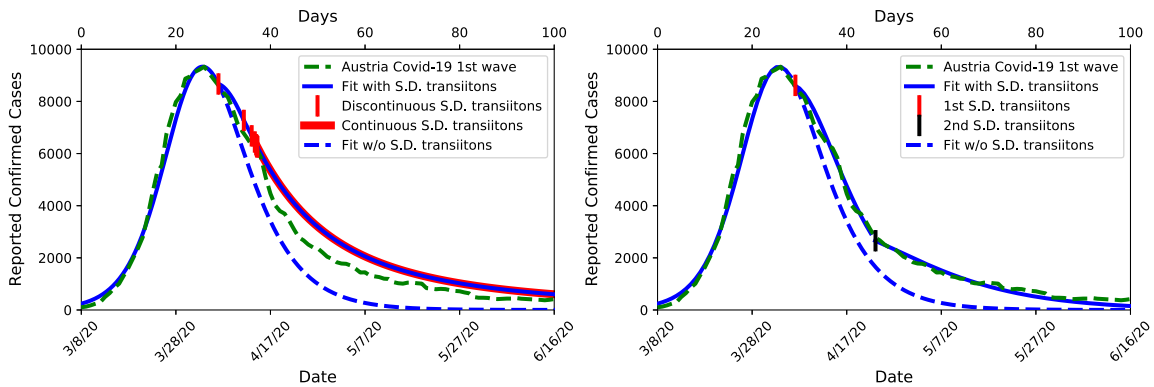

Fig. 7. Alternative fits of Austria COVID-19 first wave (A) fit with a different date for the first transition. There is a significant deviation between reported and calculated confirmed cases. This demonstrates that the fit techniques are sensitive to the choice of the first transition. This sensitivity provides a hope that the fit may reveal something about the real parameters of the population or economics of the state. (B) fit with two different distance transitions. By adjusting utility function weights $E^{(1)}, E^{(2)}$ separately for every transition a better fit can be achieved. In the case of Austria, only two transitions are required. This method is less sensitive to the choice of the first transition.

trajectories, with differences that are below resolution of this work. It is true that if the first transition occurs soon after the maximum number of infected is reached − other conditions may cause greater differences between β and γ fits.

The fit proceeds in the following steps: first, a small region around the greatest number of infected, see Fig. 6, is used to calibrate s_0, I_0, β, A. The initial value $s_{th}^{(0)} = \gamma/\beta$. During the first fit, $\gamma = 0.26$ is constant. This choice can be quite arbitrary in the boundaries of reported COVID-19 $\frac{1}{7} < \gamma \ [\text{day}^{-1}] < 1$ values [54]. We remind you that it also can be affected by contact tracing and isolation policies.

Second, one detects a discontinuous change in the time derivative of reported confirmed cases, see the outermost left red bar in Fig. 6. It defines t and s_{tr} of the first transition. New values of β and γ were fitted for a confirmed case during the period of about 20 days after the transition. In all cases, the fit predicted β to remained unchanged while γ becomes a new value. Thus $s_{th}^{(0)}$ becomes $s_{th}^{(1)}$. Third, Eq. (18) is solved for $E^{(1)}$ and $E^{(2)}$ (e.g. using the Nelder–Mead method), when $s_{tr}^{(1)}$ and $s_{th}^{(1)}$ are the values from the previous step. Fourth, next transitions $s_{tr}^{(2)}$ and $s_{th}^{(2)}$, are calculated using (18) and (19). This procedure is repeated to calculate discontinuous transitions $s_{tr}^{(k)}$ and $s_{th}^{(k)}$ till the limit s_{tr}^{lim} is reached. The continuous changes of s_{th} are calculated using (19).

To fit casualties, an effective population size N is chosen to fit reported COVID-19 deaths on the 100th day of the first wave. It predicted a quite small N less than $\frac{1}{10}$ of the Austrian population. This result will be addressed during the discussion below. Besides, there exists some time shift between calculated and reported coronavirus deaths.

The complete dynamics of the first wave confirmed cases and susceptible people, see Fig. 6, follow Eqs. (20) and the fitted $s_0, I_0, s_{th}, \beta, A, N$ together with the transitions' locations $t_i, s_{tr}^{(i)}$ and strengths s_{th}^i. See Fig. 6 for changes in s_{th}.

Two alternative fits of Austrian COVID-19 data are shown in Fig. 7. The first demonstrates the sensitivity of the fit to the choice of the first transition. The second demonstrates that for any first transition the entire curve can be fitted if $E^{(1)}, E^{(2)}$ are fitted separately.
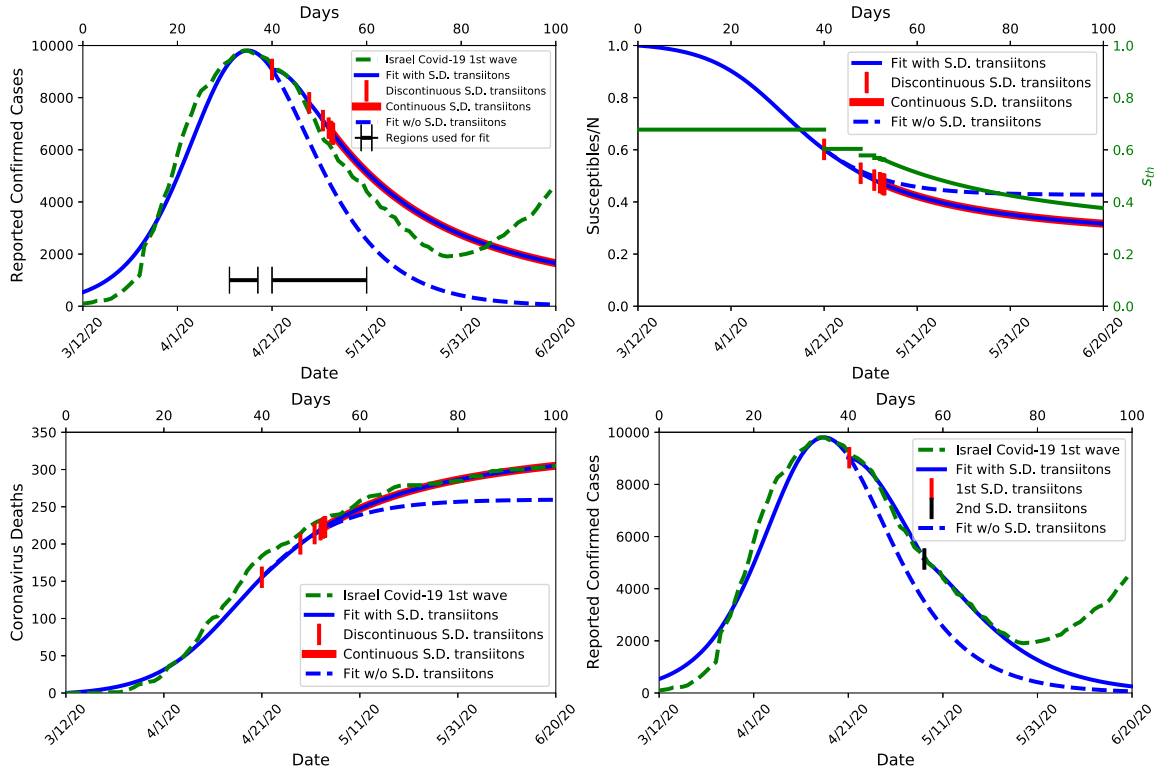
Fig. 8. Fit of Israel's COVID-19 first wave. The results are similar to the case of Austria. The fit is valid until the beginning of the second wave, at about the 70th day of the first one (A) Confirmed cases. A significant deviation exists between reported and calculated confirmed cases even before the start of the second wave. (B) Susceptible people and s_{th}. The social distancing parameter s_{th} remains a bit higher in Israel relative to Austria or Germany. (C) Coronavirus deaths. The time delay between reported and calculated cases is smaller than in the case of Austria. It can be explained either by late or early reports of coronavirus tests or reported deaths in Israel or Austria respectively. (D) Alternative fit with two transitions.

The results for Germany and Israel are summarized in Figs. 8 and 9 together with Table 1, which summarizes the results for all three countries. All countries demonstrated a low size of the effective population. One of the assumptions was that $s_0 \approx 1$. In the case of Israel, it was required to be constrained during the fit. Neither of the deviations from the fit refutes the main results of this work.

Analysis of the first wave predicts a small, less than $\frac{1}{10}$, effective population size in all three countries studied, see Table 1. An estimate of effective population size depends on the choice of M - infected fatality rate (IFR). Increase/reduction in M causes a proportional reduction/increase in effective population size N and predicted ratio A' between reported and real numbers of infected. These values in Table 1 correspond to $M = 0.1\%$. The reported value of M for Germany is 0.37% [55]. Thus N and A' maybe about $\times 4$ lower than in Table 1. Nevertheless M as low as 0.17% were reported [56]. All other predictions or results of this work, including the graphs, are independent of M. Mortality rate $M > 0.3\%$ causes non-physical $A' < 1$ in the case of Israel.

The first waves of COVID-19 in Austria, Germany, and Israel were fitted using the SIRIT model in two different ways. The first was a series of discontinuous transitions with constant economic parameters. Parameters $E^{(1)}, E^{(2)}$ were fitted by the first transition. In the second, economic weights were fitted for every candidate transition (deviation from SIR model). Both these scenarios include discontinuous changes in social distancing and possess the same first transition.

4. Discussion

This work describes Ginzburg–Landau-like instability in the SIR epidemiological model extended with time-dependent human behavior. The utility function models rational decision-making regarding the optimal level of social distancing. First, we describe the discontinuous dynamics of this model. Second, we try to show that reported infections or deaths during the COVID-19 pandemic may include the evidence of a predicted discontinuous transition. The first task allows rigorous treatment. The second task requires many assumptions that we will discuss shortly.

Let us start with a discussion of the choice of the utility function and the corresponding decision-making process. The utility function consists of two parts — the cost of the epidemic and the economic cost of social distancing.

Following several previous works, we take final epidemic size *FES* as the main cost of the epidemic. *FES* according to the SIR model in (s, i) space, in addition to the current state of the epidemic (s_t, i_t), depend on the single parameter —
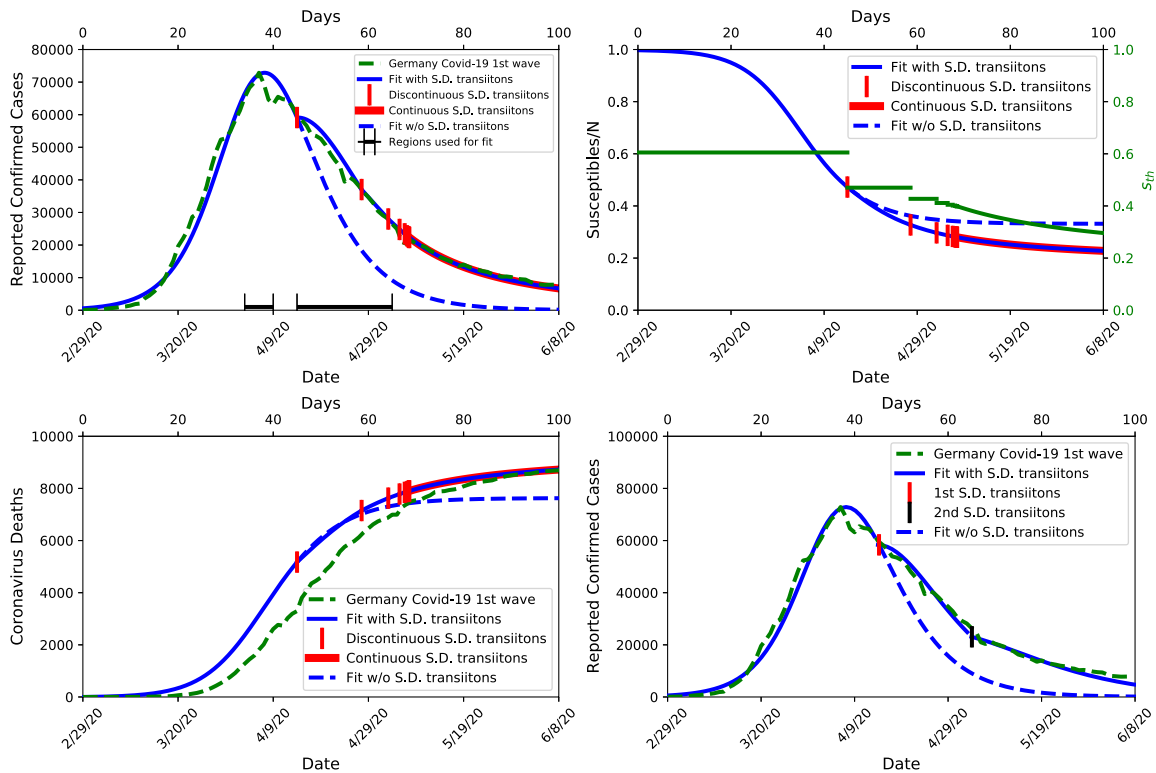
Fig. 9. Fit of Germany's COVID-19 first wave. The results are very similar to the case of Austria. (A) Confirmed cases (B) Susceptible people and s_{th} (C) Coronavirus deaths. There is a time delay between calculated and reported deaths, like in the case of Austria. (D) Alternative fit with two transitions.

Table 1

Parameters of the SIRIT model that fit the first COVID-19 wave of Austria, Germany, and Israel. The parameters may be used to reproduce the figures of the article. For the definition of parameters see Eqs. (2), (3) and (20). Besides, D_1 and D_2 are the days of the first and the second (if required) transitions. $E^{(1)}$, $E^{(2)}$ are the weights of the utility function which were fitted for the first transition. An interesting result is a small effective population size N, less than $\frac{1}{10}$ of the state population. Greater values of mortality rate M (factor k) predict even lower values of population size N (increase in M causes a proportional reduction in effective population size N and A' ratio between the real and reported number of infected). Mortality rate $M > 0.3\%$ ($k > 3$) causes non-physical $A' < 1$ in the case of Israel. The second transition in the case of Germany and Israel brings a change in β. The results of all three countries are quite similar except A' - the ratio between the real and reported number of infected people.

	s_0	i_0	γ	s_{th}	β	$s_{th}^{(1)}$	β^1	$s_{th}^{(2)}$	β^2	A	N	A'	M (IFR)	D_1	D_2	$E^{(1)}$	$E^{(2)}$
Austria, Figs. 2, 3, 6	0.99	242	0.26	0.56	0.46	0.45	0.46			1.26e−05	8.2e5/k	10/k	$k \times 10^{-3}$	32		1.31	5.81
Austria, Fig. 6A	0.99	242	0.26	0.56	0.46	0.48	0.46			1.26e−05	8.2e5/k	10/k	$k \times 10^{-3}$	29		1.84	6.30
Austria, Fig. 6B	0.99	242	0.26	0.56	0.46	0.48	0.46	0.32	0.46	1.26e−05	8.2e5/k	10/k	$k \times 10^{-3}$	29	46	1.84	6.30
Germany, Fig. 9A, B, C	0.99	578	0.26	0.60	0.43					1.24e−6	1.1e7/k	14/k	$k \times 10^{-3}$	45		1.15	5.93
Germany, Fig. 9D	0.99	578	0.26	0.60	0.43	0.47	0.43	0.33	0.52	1.24e−6	1.1e7/k	14/k	$k \times 10^{-3}$	45	65	1.15	5.93
Israel, Fig. 8A, B, C	1.0	535	0.26	0.68	0.38	0.60	0.38			6.34e−06	4.5e5/k	3/k	$k \times 10^{-3}$	40		1.33	4.92
Israel, Fig. 8D	1.0	535	0.26	0.68	0.38	0.60	0.38	0.50	0.51	6.34e−06	4.5e5/k	3/k	$k \times 10^{-3}$	40	56	1.33	4.92

basic reproduction number R_0. The price of pandemics, however, can go beyond the final epidemic size *FES*. For instance, one may include time derivatives of the number of infected people as a psychological factor that affects individual decision-making. There is a lot of room to make the utility function more complicated, but this work demonstrates that discontinuous dynamics may be achieved even with a basic model.

The economic cost is assumed to be a function of $s_{th} = 1/R_0$. Basic reproduction number $1/s_{th} = R_0$ also serve as a social distancing parameter. This choice does not change the major predictions or analytical developments of this work. In our opinion, the parameter $0 < s_{th} < 1$ that can be compared with the fraction of susceptible people in a population serves better the purpose of this work.

The main purpose of a utility function is to represent decision making. This work assumes that decision-making considers every transition $s_{th}^{(k)} \rightarrow s_{th}^{(k+1)}$ as a single one, suggesting that the new value $s_{th}^{(k+1)}$ preserves till the end of epidemic. This is a major assumption of this work because elaborate decision-making should consider future possible changes in $s_{th}^{(k+1)}$.

The specific choice of the utility function makes it possible rigorous treatment of a single transition of social distancing. Multiple transitions require additional assumptions around economic costs which change from transition to transition. The economic cost is assumed to be constant with time during the fit of COVID-19 data.

The ratio between total and confirmed infected A', population size N, and infected fatality rate (IFR) M are assumed to be constant during the first wave of COVID-19. It is a very strong assumption, especially regarding the A', which depends on the number of tests. Nevertheless, one can hope that A' preserves for some time while test policies are the same. Especially important for this work is the time from the maximum number of infected till the first predicted transition, see Fig. 6.

All these assumptions provided a successful fit of COVID-19 data in Austria, Germany, and Israel. Austria and Israel are countries with similar population sizes and with similar policies during the initial stages of the first wave. Germany is a country with a population of about $\times 10$ the size of the other two countries, which still demonstrated SIR-like behavior during the first wave.

All three countries studied entered a transition soon after the epidemic started to decline. During the fit, this work cannot distinguish between the transition of social distancing s_{th} and changes in parameters that were assumed to be constant, for instance, A'. Thus, transition in social distancing remains a hypothesis.

An interesting conclusion of the fit is that the first transition of social distancing $s_{th}^{(0)} \rightarrow s_{th}^1$ corresponds to the change of γ rather than β. β remains constant during the first transition of $s_{th} = \gamma/\beta$. Generally, human behavior is associated with changes in β that are directly connected to the frequency of interactions and behavior during such interactions. Nevertheless, during extreme events such as COVID-19, the contagious period γ^{-1} can be shortened due to contact tracing and the isolation of the confirmed or possibly infected. Some studies highlight the importance of γ changes [57]. It is important to state that the general theory of social distancing transitions in Section 2 is not affected by this finding.

A small effective population size during the first wave is another surprising result of the fit. An explanation of low N may be that the initial lockdown separated the population in disconnected domains [58,59] and the wave of the epidemic occurred in a limited number of domains. The other possible explanation is that a significant part of the population is immune to COVID-19 [60]. Finally, the SIR approach is an oversimplified presentation of reality.

The small effective population size during the first wave may indicate a danger of an abrupt transition to a bigger population size when s_{th} reduces below some critical value. It may result in a significant second wave of the epidemic. It depends on the network structure of the population.

The SIR model can be mapped on percolation in an Erdos–Renyi network [61]. *FES* corresponds to a giant component in percolation models. The critical value of the basic reproduction number for a percolation transition was reported for some interaction networks [59,62–64], though scale-free networks lack it [58]. Future work may extend these tools to calculate the derivatives of *FES* (11) to the general derivatives of giant components in percolation models.

Network theory may help to set the validity boundaries of this work. For instance, the predictions of this work may become invalid if the parameter of social distancing is a function $f(R_0)$ such that *FES* as a function of f ceases to be non-linear. An example of such a function is the transmission $T = 1 - \exp(-1/s_{th})$ in a scale-free network [64].

There are alternative explanations to discontinuities in observed COVID-19 data, for instance, government regulations [65] or continuous exogenous phenomena [66]. Relative weights of government regulations and individual decision-making regarding social distancing cannot be addressed in the framework of this work. Nevertheless, testing the basic decision-making model against real data is important. The evolution of decision-making could converge to some basic model which is different from complex modern reality.

To conclude, this work predicts observable discontinuous transitions of social distancing and provides tools for quantitative analysis of pandemic waves. The dynamics include the Zeno-like effect of infinite transitions during a finite time. Multiple transitions may be interesting for theories of crisis formation — the probability that something goes wrong increases with the number of decision points. The developed tools contributing to social epidemiology, like the SIR model, may be mapped to network percolation theory and the spread of non-contagious but going-viral phenomena [67,68].

CRediT authorship contribution statement

R. Arazi: Performed research, Wrote paper. **A. Feigel:** Performed research, Wrote paper.

Declaration of competing interest

The authors declare that they have no known competing financial interests or personal relationships that could have appeared to influence the work reported in this paper.

Appendix A. Analytic solution of (3)

The first two equations of (2) may be rewritten as:

$$\frac{1}{\beta}\frac{\partial z}{\partial x}z = -\beta\left(s_{th} + \frac{1}{\beta}z\right)\exp(x), \tag{A.1}$$

using transformation $\frac{\partial \log i}{\partial t} = z$, $\frac{\partial z}{\partial t} = \frac{\partial z}{\partial \log i} \frac{\partial \log i}{\partial t} = \frac{\partial z}{\partial \log i} z$, $x = \log i$. Integration of (A.1) results in:

$$i = i_0 + \left[s_0 - s + s_{th} \log \left[\frac{s}{s_0} \right] \right], \tag{A.2}$$

where (s_0, i_0) are initial values of s and i.

The time between current value s and s_{tr} is:

$$\int_s^{s_{tr}} \frac{ds}{\frac{ds}{dt}} = \int_s^{s_{tr}} \frac{ds}{-\beta \left[i_0 + \left[s_0 - s + s_{th} \log \left[\frac{s}{s_0} \right] \right] \right] s}, \tag{A.3}$$

and remain finite while $s_{tr} > s_{min}$.

To derive s in the form of the Lambert W function (defined as $W(x)$, where $W \exp W = x$) one should rewrite (A.2) as:

$$-\frac{s}{s_{th}} \exp \left[-\frac{s}{s_{th}} \right] = -\frac{s_0}{s_{th}} \exp \left[\frac{(i - i_0) - s_0}{s_{th}} \right]. \tag{A.4}$$

The expressions (A.4) and (A.2) provide connections between s and i along the population trajectory in (s, i) space that initiates at (s_0, i_0). Lambert W function should be used carefully because it is a multi-valued function.

Let us define by (s_t, i_t) the values of the susceptible ratio s and the number of infected i along the population trajectory in (s, i) space that initiates at (s_0, i_0). Then let us calculate the coefficients $F^{(1)}$, $F^{(2)}$, $F^{(3)}$ (10) and show that along trajectory (s_t, i_t) they are polynomials of $\log[s_t]$. Derivatives of $\log[s_{min}]$:

$$\log[s_{min}] = \log[s_{th}] + \log[W(f(s_{th}))], \tag{A.5}$$

due to s_{th} include derivatives of $\log[s_{th}]$ and derivatives of $\log[W(f(s_{th}))]$, where:

$$f(s_{th}) = -\frac{s_0}{s_{th}} \exp \left[-\frac{s_0 + i_0}{s_{th}} \right]. \tag{A.6}$$

Let us notice that s_{th}, $f(s_{th})$ and $W(f(s_{th}))$ are constant along trajectory (s_t, i_t) until the value of s_{th} changes by a transition. The values $f(s_{th})$ and $W(f(s_{th}))$:

$$f = -\frac{s_0}{s_{th}} \exp \left[-\frac{s_0}{s_{th}} - \frac{i_0}{s_{th}} \right], \tag{A.7}$$

$$W(f) \qquad = -\frac{s_{min}}{s_{th}}, \tag{A.8}$$

are constant until a transition takes place, because s_{min} (A.5) is constant along the trajectory unless s_{th} changes its value. Besides:

$$-\frac{s_0}{s_{th}} \exp \left[-\frac{i_0 + s_0}{s_{th}} \right] = \left(-\frac{s_t}{s_{th}} \exp \left[-\frac{s_t}{s_{th}} - \frac{i_t}{s_{th}} \right] \right) = const, \tag{A.9}$$

because any point (s_t, i_t) can serve as an initial value (s_0, i_0) for the continuation of the trajectory.

Derivatives of $\log[s_{th}]$ depend only on s_{th} and, so, are constant until s_{th} changes.

Derivatives of $\log[W(f(s_{th}))]$ are:

$$\frac{d \log W(f)}{ds_{th}} = \frac{d \log W(f)}{df} \frac{df}{ds_{th}}$$

$$\frac{d^2 \log W(f)}{ds_{th}^2} = \frac{d^2 \log W(f)}{df^2} \left(\frac{df}{ds_{th}} \right)^2 + \frac{d \log W(f)}{df} \frac{d^2 f}{ds_{th}^2}$$

$$\frac{d^3 \log W(f)}{ds_{th}^3} = \frac{d^3 \log W(f)}{df^3} \left(\frac{df}{ds_{th}} \right)^3 +$$

$$3 \frac{d^2 \log W(f)}{df^2} \frac{df}{ds_{th}} \frac{d^2 f}{ds_{th}^2} + \frac{d \log W(f)}{df} \frac{d^3 f}{ds_{th}^3} \tag{A.10}$$

Derivatives of $\log W(f)$ due to f are invariant along (s_t, i_t) trajectory, see Appendix B.

Derivatives of f due to s_{th} are polynomials of $\log[s_t]$. Consider the first derivative of (A.6) taking into account (A.9):

$$\frac{df}{ds_{th}} = gf, \tag{A.11}$$

where:

$$g = \left(-\frac{1}{s_{th}} \right) + \left(\frac{s_t + i_t}{s_{th}^2} \right). \tag{A.12}$$

Expression (A.2) can be rewritten in the form:

$$i_t + s_t = i_0 + s_0 + s_{th} \log \left[\frac{s_t}{s_0} \right] \tag{A.13}$$

for trajectory (s_t, i_t). Plugging (A.13) in (A.12) results in:

$$g = \left[\left(-\frac{1}{s_{th}} \right) + \left(\frac{i_0 + s_0 + s_{th} \log \left[\frac{s_t}{s_0} \right]}{s_{th}^2} \right) \right]. \tag{A.14}$$

Thus g and its derivatives due to s_{th} are linear functions of $\log[s_t]$. The second and the third derivatives then:

$$\frac{d^2 f}{ds_{th}^2} = fg^2 + f \frac{dg}{ds_{th}} \tag{A.15}$$

$$\frac{d^3 f}{ds_{th}^3} = fg^3 + 3fg \frac{dg}{ds_{th}} + f \frac{d^2 g}{ds_{th}^2} \tag{A.16}$$

are the quadratic and cubic polynomials of $\log[s_t]$.

Appendix B. Derivatives of the Lambert W function

All derivatives of W due to f are constant along any trajectory in (s, i) space:

$$W \exp[W] = f, \tag{B.1}$$

$$\frac{d \log W}{df} = \frac{1}{f(1+W)}, \tag{B.2}$$

$$\frac{d^2 \log W}{df^2} = -\frac{1}{f} \frac{d \log W}{df} - fW \left[\frac{d \log W}{df} \right]^3, \tag{B.3}$$

$$\frac{d^3 \log W}{df^3} = \frac{1}{f^2} \frac{d \log W}{df} - \frac{1}{f} \frac{d^2 \log W}{df^2} - W \left[\frac{d \log W}{df} \right]^3 - fW \left[\frac{d \log W}{df} \right]^4 - 3fW \left[\frac{d \log W}{df} \right]^2 \frac{d^2 \log W}{df^2}. \tag{B.4}$$

The final expressions are invariant until s_{th} changes because they depend on f and W only, see (A.8).

Appendix C. Expressions for $F^{(1)}$, $F^{(2)}$ and $F^{(3)}$

The first:

$$F^{(1)} = -\frac{i_0 - s_{min} + s_{th} \log \left(\frac{s}{s_0} \right) + s_0}{s_{th} (s_{th} - s_{min})} \tag{C.1}$$

The second:

$$F^{(2)} = -\frac{1}{2s_{th}^2 (s_{th} - s_{min})^3} \times \tag{C.2}$$

$$\left(i_0 - s_{min} + s_{th} \log \left(\frac{s}{s_0} \right) + s_0 \right) \times$$

$$\left(s_{min} (i_0 - s_{min} + s_0) + 2s_{min}s_{th} + s_{min}s_{th} \log \left(\frac{s}{s_0} \right) - 2s_{th}^2 \right)$$

and

$$F^{(3)} = -\frac{1}{6s_{th}^3 (s_{th} - s_{min})^5} \left(i_0 - s_{min} + s_{th} \log \left(\frac{s}{s_0} \right) + s_0 \right) \left[\left(-3s_{min}s_{th}^2 (3i_0 - 5s_{min} + 3s_0) \right) + \right.$$

$$\left. s_{min}s_{th} (i_0 - s_{min} + s_0)(i_0 + 8s_{min} + s_0) + s_{min}s_{th} \log \left(\frac{s}{s_0} \right) \times \right. \tag{C.3}$$

$$\left(s_{\text{th}} \left(2i_0 + 7s_{\text{min}} + 2s_0 \right) + 4s_{\text{min}} \left(i_0 - s_{\text{min}} + s_0 \right) + s_{\text{th}} \log \left(\frac{s}{s_0} \right) \left(2s_{\text{min}} + s_{\text{th}} \right) - 9s_{\text{th}}^2 \right) + $$

$$2s_{\text{min}}^2 \left(i_0 - s_{\text{min}} + s_0 \right)^2 - 12 s_{\text{min}} s_{\text{th}}^3 + 6 s_{\text{th}}^4 \Bigg]$$

where s_{min} is defined by (A.5).

Expressions developed in appendices use the parameters of the SIR model Eqs. (2). Transformation $i \rightarrow AI$ converts previous equations to the parameters of (20).

References

[1] R.M. May, R.M. Anderson, The transmission dynamics of human immunodeficiency virus (HIV), Philos. Trans. R. Soc. London [Biol] 321 (1207) (1988) 565–607.
[2] R.M. Anderson, H. Heesterbeek, D. Klinkenberg, T.D. Hollingsworth, How will country-based mitigation measures influence the course of the COVID-19 epidemic? Lancet 395 (10228) (2020) 931.
[3] A. Atkeson, 2020, [link]. URL http://www.nber.org/papers/w26867.pdf.
[4] M. Farboodi, G. Jarosch, R. Shimer, Internal and external effects of social distancing in a pandemic, 2020, URL https://www.nber.org/papers/w27059.pdf.
[5] F. Alvarez, 2020, [link]. URL https://www.nber.org/papers/w26981.pdf.
[6] V. Capasso, G. Serio, A generalization of the Kermack-McKendrick deterministic epidemic model, Math. Biosci. 42 (1) (1978) 43–61.
[7] L.D. Landau, E.M. Lifshitz, Statistical Physics: Volume 5, Vol. 5, Elsevier, 2013.
[8] M. Perc, Phase transitions in models of human cooperation, Phys. Lett. A 380 (36) (2016) 2803–2808.
[9] M. Levy, Social phase transitions, J. Econ. Behav. Organ. 57 (1) (2005) 71–87.
[10] J.A. Kelso, Phase transitions and critical behavior in human bimanual coordination, Am. J. Phys. Reg. 246 (6) (1984) R1000–R1004.
[11] J.M. Encinas, P.E. Harunari, M.M. de Oliveira, C.E. Fiore, Fundamental ingredients for discontinuous phase transitions in the inertial majority vote model, Sci. Rep. 8 (1) (2018).
[12] P.A. Diamond, E. Maskin, An equilibrium analysis of search and breach of contract, i: Steady states, Bell J. Econ. 10 (1) (1979) 282.
[13] N. Ferguson, Capturing human behaviour, Nature 446 (7137) (2007) 733.
[14] C. Bauch, A. d'Onofrio, P. Manfredi, Behavioral epidemiology of infectious diseases: An overview, in: P. Manfredi, A. D'Onofrio (Eds.), Modeling the Interplay Between Human Behavior and the Spread of Infectious Diseases, Springer, 2013, pp. 1–19.
[15] E.O. Jordan, et al., Epidemic influenza. a survey, in: Epidemic Influenza. A Survey, 1927.
[16] G. Chowell, L. Bettencourt, N. Johnson, W. Alonso, C. Viboud, The 1918–1919 influenza pandemic in england and wales: Spatial patterns in transmissibility and mortality impact, Proc. Biol. Sci. 275 (2008) 501–509.
[17] W.O. Kermack, A.G. McKendrick, A contribution to the mathematical theory of epidemics, Proc. R. Soc. Lond. Ser. A Math. Phys. Eng. Sci. 115 (772) (1927) 700–721.
[18] S. Del Valle, H. Hethcote, J. Hyman, C. Castillo-Chavez, Effects of behavioral changes in a smallpox attack model, Math. Biosci. 195 (2) (2005) 228–251.
[19] E.P. Fenichel, Economic considerations for social distancing and behavioral based policies during an epidemic, J. Health Econ. 32 (2) (2013) 440–451.
[20] E.P. Fenichel, C. Castillo-Chavez, M.G. Ceddia, G. Chowell, P.A.G. Parra, G.J. Hickling, G. Holloway, R. Horan, B. Morin, C. Perrings, M. Springborn, L. Velazquez, C. Villalobos, Adaptive human behavior in epidemiological models, Proc. Natl. Acad. Sci. 108 (15) (2011) 6306–6311.
[21] M. Kremer, Integrating behavioral choice into epidemiological models of aids, Quat. J. Econ. 111 (2) (1996) 549–573.
[22] A. d'Onofrio, P. Manfredi, Information-related changes in contact patterns may trigger oscillations in the endemic prevalence of infectious diseases, J. Theoret. Biol. 256 (3) (2009) 473–478.
[23] M. Kochanczyk, F. Grabowski, T. Lipniacki, Dynamics of COVID-19 pandemic at constant and time dependent contact rates, Math. Model. Nat. Phenom. 15 (2020).
[24] A. d'Onofrio, M. Banerjee, P. Manfredi, Spatial behavioural responses to the spread of an infectious disease can suppress turing and turing-hopf patterning of the disease, Phys. A 545 (2020).
[25] P. van den Driessche, J. Watmough, A simple SIS epidemic model with a backward bifurcation, J. Math. Biol. 40 (6) (2000) 525–540.
[26] G.O. Agaba, Y.N. Kyrychko, K.B. Blyuss, Mathematical model for the impact of awareness on the dynamics of infectious diseases, Math. Biosci. 286 (2017) 22–30.
[27] W. Wang, Modeling adaptive behavior in influenza transmission, Math. Model. Nat. Phenom. 7 (3) (2012) 253–262.
[28] B. Buonomo, A. d'Onofrio, D. Lacitignola, Globally stable endemicity for infectious diseases with information-related changes in contact patterns, Appl. Math. Lett. 25 (7) (2012) 1056–1060.
[29] G. Liu, Z. Liu, Z. Jin, Dynamics analysis of epidemic and information spreading in overlay networks, J. Theoret. Biol. 444 (2018) 28–37.
[30] C. Vargas-De-Leon, A. D' Onofrio, Global stability of infectious disease models with contact rate as a function of prevalence index, Math. Biosci. Eng. 14 (4) (2017) 1019–1033.
[31] D. McAdams, Nash SIR: An economic-epidemiological model of strategic behavior during a viral epidemic, 2020, arXiv:2006.10109 [econ].
[32] M. Eichenbaum, S. Rebelo, M. Trabandt, 2020, [link]. URL http://www.nber.org/papers/w26882.pdf.
[33] F. Toxvaerd, 2020, [link]. URL http://www.econ.cam.ac.uk/research-files/repec/cam/pdf/cwpe2021.pdf.
[34] S. Hur, M. Jenuwine, Lessons on the economics of pandemics from recent research, Econ. Comm. (2020) publisher: Federal Reserve Bank of Cleveland (2020).
[35] M.G. Ceddia, N.O. Bardsley, R. Goodwin, G.J. Holloway, G. Nocella, A. Stasi, A complex system perspective on the emergence and spread of infectious diseases: Integrating economic and ecological aspects, Ecol. Econom. 90 (2013) 124–131.
[36] B.R. Morin, E.P. Fenichel, C. Castillo-Chavez, SIR dynamics with economically driven contact rates, Nat. Resour. Model. 26 (4) (2013) 505–525.
[37] S. Bhattacharyya, T. Reluga, Game dynamic model of social distancing while cost of infection varies with epidemic burden, IMA J. Appl. Math. 84 (1) (2019) 23–43.
[38] R. Elie, E. Hubert, G. Turinici, Contact rate epidemic control of COVID-19: an equilibrium view, Math. Model. Nat. Phenom. 15 (2020).
[39] T.C. Reluga, Game theory of social distancing in response to an epidemic, PLoS Comput. Biol. 6 (5) (2010) e1000793.
[40] N.M. Ferguson, M.J. Keeling, W.J. Edmunds, R. Gani, B.T. Grenfell, R.M. Anderson, S. Leach, Planning for smallpox outbreaks, Nature 425 (6959) (2003) 681–685.

[41] P. Poletti, B. Caprile, M. Ajelli, A. Pugliese, S. Merler, Spontaneous behavioural changes in response to epidemics, J. Theoret. Biol. 260 (1) (2009) 31–40.
[42] Z. Wang, M.A. Andrews, Z.-X. Wu, L. Wang, C.T. Bauch, Coupled disease - behavior dynamics on complex networks: A review, Phys. Life Rev. 15 (2015) 1–29.
[43] P.C. Ventura da Silva, F. Velasquez-Rojas, C. Connaughton, F. Vazquez, Y. Moreno, F.A. Rodrigues, Epidemic spreading with awareness and different timescales in multiplex networks, Phys. Rev. E 100 (3) (2019).
[44] K. Janssen, H. Komen, H.W. Saatkamp, M.C.M. de Jong, P. Bijma, Derivation of the economic value of R0 for macroparasitic diseases and application to sea lice in salmon, Genet. Select Evol. 50 (1) (2018) 47.
[45] O. Diekmann, J.A.P. Heesterbeek, J.A. Metz, On the definition and the computation of the basic reproduction ratio R0 in models for infectious diseases in heterogeneous populations, J. Math. Biol. 28 (4) (1990) 365–382.
[46] J. Tanimoto, Social dilemma analysis of the spread of infectious disease, in: Evol. Games Sociophys., Vol. 17, 2018, pp. 155–216.
[47] K. Kuga, J. Tanimoto, M. Jusup, To vaccinate or not to vaccinate: A comprehensive study of vaccination-subsidizing policies with multi-agent simulations and mean-field modeling, J. Theoret. Biol. 469 (2019) 107–126.
[48] J. Lehtonen, The Lambert W function in ecological and evolutionary models, Methods Ecol. Evol. 7 (9) (2016) 1110–1118.
[49] F. Wang, Application of the Lambert *W* function to the SIR epidemic model, College Math. J. 41 (2) (2010) 156–159.
[50] T. Reluga, A two-phase epidemic driven by diffusion, J. Theoret. Biol. 229 (2) (2004) 249–261.
[51] T. Britton, Stochastic epidemic models: A survey, Math. Biosci. 225 (1) (2010) 24–35.
[52] E. Dong, H. Du, L. Gardner, An interactive web-based dashboard to track COVID-19 in real time, Lancet Infect. Dis. 20 (5) (2020) 533–534.
[53] J. Mossong, N. Hens, M. Jit, P. Beutels, K. Auranen, R. Mikolajczyk, M. Massari, S. Salmaso, G.S. Tomba, J. Wallinga, J. Heijne, M. Sadkowska-Todys, M. Rosinska, W.J. Edmunds, Social contacts and mixing patterns relevant to the spread of infectious diseases, Plos Med. 5 (3) (2008) 381–391.
[54] M.M. Bohmer, U. Buchholz, V.M. Corman, M. Hoch, K. Katz, D.V. Marosevic, S. Bohm, T. Woudenberg, N. Ackermann, R. Konrad, U. Eberle, B. Treis, A. Dangel, K. Bengs, V. Fingerle, A. Berger, S. Hörmansdorfer, S. Ippisch, B. Wicklein, A. Grahl, K. Pörtner, N. Muller, N. Zeitlmann, T.S. Boender, W. Cai, A. Reich, M. an der Heiden, U. Rexroth, O. Hamouda, J. Schneider, T. Veith, B. Muhlemann, R. Wolfel, M. Antwerpen, M. Walter, U. Protzer, B. Liebl, W. Haas, A. Sing, C. Drosten, A. Zapf, Investigation of a COVID-19 outbreak in germany resulting from a single travel-associated primary case: a case series, Lancet Infect. Dis. 20 (8) (2020) 920–928.
[55] H. Streeck, B. Schulte, B. Kuemmerer, E. Richter, T. Hoeller, C. Fuhrmann, E. Bartok, R. Dolscheid, M. Berger, L. Wessendorf, M. Eschbach-Bludau, A. Kellings, A. Schwaiger, M. Coenen, P. Hoffmann, M. Noethen, A.-M. Eis-Huebinger, M. Exner, R. Schmithausen, M. Schmid, G. Hartmann, (2020).
[56] E. Bendavid, B. Mulaney, N. Sood, S. Shah, E. Ling, R. Bromley-Dulfano, C. Lai, Z. Weissberg, R. Saavedra-Walker, J. Tedrow, D. Tversky, A. Bogan, T. Kupiec, D. Eichner, R. Gupta, J. Ioannidis, J. Bhattacharya, (2020).
[57] J. Gans, The economic consequences of R = 1, Covid Econ. (2020) 28.
[58] D.S. Callaway, M.E.J. Newman, S.H. Strogatz, D.J. Watts, Network robustness and fragility: Percolation on random graphs, Phys. Rev. Lett. 85 (25) (2000) 4.
[59] C. Warren, L. Sander, I. Sokolov, Geography in a scale-free network model, Phys. Rev. E 66 (5) (2002).
[60] J. Mateus, A. Grifoni, A. Tarke, J. Sidney, S.I. Ramirez, J.M. Dan, Z.C. Burger, S.A. Rawlings, D.M. Smith, E. Phillips, S. Mallal, M. Lammers, P. Rubiro, L. Quiambao, A. Sutherland, E.D. Yu, R. da Silva Antunes, J. Greenbaum, A. Frazier, A.J. Markmann, L. Premkumar, A. de Silva, B. Peters, S. Crotty, A. Sette, D. Weiskopf, Selective and cross-reactive SARS-CoV-2 t cell epitopes in unexposed humans, Science (2020) 3871.
[61] P. Grassberger, On the critical-behavior of the general epidemic process and dynamical percolation, Math. Biosci. 63 (2) (1983) 157–172.
[62] L. Sander, C. Warren, I. Sokolov, C. Simon, J. Koopman, Percolation on heterogeneous networks as a model for epidemics, Math. Biosci. 180 (1–2) (2002) 293–305.
[63] M. Newman, The structure and function of complex networks, SIAM Rev. 45 (2) (2003) 167–256.
[64] M.E.J. Newman, Spread of epidemic disease on networks, Phys. Rev. E 66 (1) (2002).
[65] L. Lopez, X. Rodo, Nat. Hum. Behav. 4 (7) (2020) 746–755.
[66] D. Earn, P. Rohani, B. Bolker, B. Grenfell, A simple model for complex dynamical transitions in epidemics, Science 287 (5453) (2000) 667–670.
[67] R.J. Shiller, Narrative economics, Amer. Econ. Rev. 107 (4) (2017) 967–1004.
[68] C.T. Bauch, A.P. Galvani, Social factors in epidemiology, Science 342 (6154) (2013) 47–49.